Combining flat crystals, bent crystals and compound refractive lenses for high-energy X-ray optics

S. D. Shastri

Advanced Photon Source, Argonne National Laboratory, Argonne, IL 60439, USA. E-mail: shastri@aps.anl.gov

Compound refractive lenses (CRLs) are effective for collimating or focusing high-energy X-ray beams (50–100 keV) and can be used in conjunction with crystal optics in a variety of configurations, as demonstrated at the 1-ID undulator beamline of the Advanced Photon Source. As a primary example, this article describes the quadrupling of the output flux when a collimating CRL, composed of cylindrical holes in aluminium, is inserted between two successive monochromators, *i.e.* a modest-energy-resolution premonochromator followed by a high-resolution monochromator. The premonochromator is a cryogenically cooled divergence-preserving bent double-Laue Si(111) crystal device delivering an energy width $\Delta E/E \simeq 10^{-3}$, which is sufficient for most experiments. The high-resolution monochromator is a four-reflection flat Si(111) crystal system resembling two channel-cuts in a dispersive arrangement, reducing the bandwidth to less than 10^{-4}, as required for some applications. Tests with 67 and 81 keV photon energies show that the high-resolution monochromator, having a narrow angular acceptance of a few microradians, exhibits a fourfold throughput enhancement due to the insertion of a CRL that reduces the premonochromatized beam's vertical divergence from 29 μrad to a few microradians. The ability to focus high-energy X-rays with CRLs having long focal lengths (tens of meters) is also shown by creating a line focus of 70–90 μm beam height in the beamline end-station with both the modest-energy-resolution and the high-energy-resolution monochromatic X-rays.

Keywords: high-energy X-rays; X-ray optics; refractive lenses; high-resolution X-ray monochromators.

1. Overview

A liquid-nitrogen-cooled monochromator for high-energy X-rays (50–200 keV) consisting of two bent Si(111) Laue crystals arranged to sequential Rowland conditions (Fig. 1) has been in operation for three years at the XOR Sector 1 undulator beamline of the Advanced Photon Source (APS). In the routinely used energy range of 60–100 keV, this monochromator delivers over ten times more flux than does a Si(111) flat-crystal monochromator, without any increase in energy width ($\Delta E/E \simeq 10^{-3}$). The bent double-Laue optics is also characterized by a fully tunable fixed-exit beam with preserved source brilliance (divergence and size). Details of the design, properties, and performance of this instrument appeared in a recent article (Shastri *et al.*, 2002). The modest 10^{-3} level of energy spread is acceptable for numerous high-energy experiments currently performed at beamline 1-ID, such as pair-distribution function measurements (Badyal *et al.*, 1997, 2002; Petkov *et al.*, 2000, 2001), fluorescence spectroscopy (Curry *et al.*, 2001, 2003), powder diffraction (Kramer *et al.*, 2002; Wilkinson *et al.*, 2002), material stress/texture determination (Wang *et al.*, 2002), small-angle scattering (Almer *et al.*, 2003), and diffuse scattering (Welberry *et al.*, 2003). Nevertheless, applications exist that require better monochromaticity ($\Delta E/E \leq 10^{-4}$). Examples include anomalous scattering with heavy elements, high-resolution stress/strain measurements with line-shape analysis, atomic physics spectroscopy, and excitation of nuclear resonances. The energy resolution of this monochromator can indeed be improved to 10^{-4} levels or better by careful choice of Laue crystal parameters, such as thickness, asymmetry, and reflection order. However, higher resolutions at high X-ray energies demand excellent mechanical stability, which is difficult to achieve at the white-beam optics stage, wherein small angular instabilities or drifts, $\delta\theta$, arising from thermal load and cooling are amplified into large energy changes, $\delta E = E \cot\theta\, \delta\theta$, as a result of the small Bragg angle, θ, and large energy, E. Narrower energy resolution might best be attained by alternatively using additional post-monochromatization optics after the broader bandwidth double-Laue system. This method keeps the white-beam optics invariant and relatively simple, and permits the subsequent high-resolution system to operate without thermal load in a more amenable and accessible open room environment, where it can be easily modified. Furthermore, it is possible to return to the configuration that uses just the high-flux modest-energy-resolution X-rays from the premonochromator by bypassing the post-monochromator. Hence, because of its versatility, this approach was pursued, and the reporting of its demonstration forms the bulk of this article. Specifically, compound refractive lenses (CRLs, shown in Fig. 2), originally conceived as focusing optics (Snigirev *et al.*, 1996; Lengeler *et al.*, 1999), were used to collimate vertically the exit beam from the double-Laue system to divergences comparable to the small angular acceptance of subsequent high-resolution flat-crystal optics (Fig. 6). This approach was suggested by the work of Baron *et al.* (1999), which examined compound refractive lenses as collimators at lower X-ray energies. The flux after the four-reflection high-resolu-

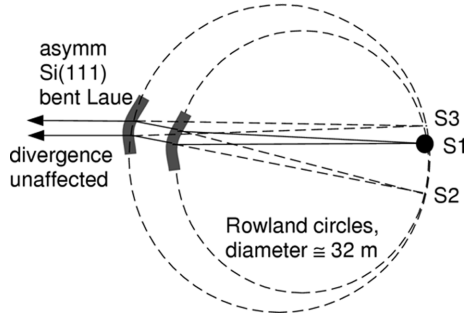

Figure 1
Tunable in-line monochromator of two vertically diffracting bent Laue crystals located ∼32 m from the undulator source, *S*1. The two Rowland circles intersect tangentially at the virtual source, *S*2.

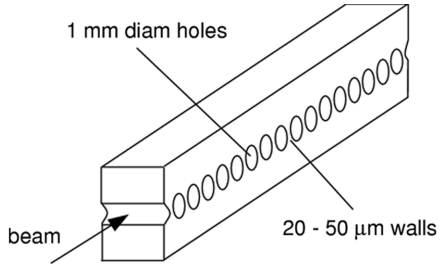

Figure 2
Sketch, with relevant dimensions, of the aluminium CRLs used here (from Adelphi Technology Inc., Palo Alto, CA, USA, http://www.adelphitech.com). X-rays propagating through many concave walls experience convergence. For example, 60 and 86 double-concave walls of 0.5 mm radius of curvature compose a 35 m-focal-length device for 67 and 81 keV X-rays, respectively.

  DOI: 10.1107/S0909049503023586

tion system is improved by a factor of four owing to the insertion of a collimating aluminium CRL, according to tests conducted with 67 and 81 keV X-rays. With a CRL in place, we obtain approximately 10^{11} photons s^{-1} in a 7×10^{-5} bandwidth in a 2×0.5 mm beam size (horizontal $\times$ vertical) at a distance of 60 m from the source. This setup has been used for resonant powder diffraction studies near the Pb and Bi *K*-edges at 88–91 keV (Shastri *et al.*, 2004).

§§2 and 3 describe the properties of the bent double-Laue premonochromator and the collimating CRLs, respectively. The performance analysis of the full high-energy-resolution setup, including the post-monochromator, is presented in §4. §5 describes the results of additional configurations involving focusing with CRLs in a roughly 1:1 geometric ratio, producing line foci with beams of both modest and high energy resolution. Finally, possible technical enhancements for the optics tested here are discussed in §6. Potential improvements include state-of-the-art CRLs developed by other researchers and further optimized high-resolution monochromators.

2. Bent double-Laue premonochromator

A detailed description of the cryogenically cooled, bent, double-Laue optics has already been given by Shastri *et al.* (2002). Its main aspects are recapitulated in this section, along with some simple ray-propagation data to demonstrate the important characteristic (Lienert *et al.*, 2001) of preserving beam brilliance (divergence and size), a feature necessary to permit successful subsequent beam manipulation by coherence/brilliance-prerequisite optics such as CRLs or Fresnel zone plates. The reason for adopting such a scheme over the more conventional geometry composed of two flat parallel crystals [*e.g.* Si(111)] is that the latter concept is inefficient at high X-ray energies. The bent Laue system provides over an order of magnitude more flux without an increase in energy spread. This more than tenfold flux enhancement results from the bending strain-induced broadening of the crystal reflection's angular acceptance (Suortti & Schulze, 1995). Concomitant with this angular broadening is an increased intrinsic bandwidth (*i.e.* the energy spread selected out of a single polychromatic incident ray). However, the impact of this increased bandwidth is neutralized by bending the crystals towards the source, with bend radii properly adjusted so that all rays make the same incidence angle with respect to the crystal planes (the so-called Rowland condition). The result is an energy spread comparable to that arising from the flat-crystal scheme. As shown in Fig. 1, the white beam is incident on the first Laue crystal, cylindrically bent to a Rowland circle going through the source, *S*1. The singly diffracted beam emerges as if emanating directly from a virtual source, *S*2, also located on the first Rowland circle. To restore the beam parallel to the original direction and provide a tunable in-line system, a second crystal is introduced that is also bent, but to a Rowland circle passing through the virtual source *S*2. The doubly diffracted beam propagates as if coming from the virtual source *S*3, located on the second Rowland circle and close to the original source, *S*1. In the actual system, both crystals are 2.5 mm thick, with surface cuts relative to the Si(111) planes selected 10° off the symmetric Laue orientation, and are bent to radii approximately equal to the 32 m distance from the undulator source. The result is a premonochromatized beam bandwidth of approximately 1.5×10^{-3} in the 60–80 keV energy range, with fluxes of $\sim 10^{12}$ photons s^{-1} mm^{-2} at the experimental end-station 60 m from the source.

The claim that the premonochromator optics leave the ray propagation from the source undisturbed was verified to a reasonable level by comparing horizontal and vertical beam profiles at different locations and examining whether the sizes scaled with the distances from the source. Figs. 3 and 4 show the results of such measurements

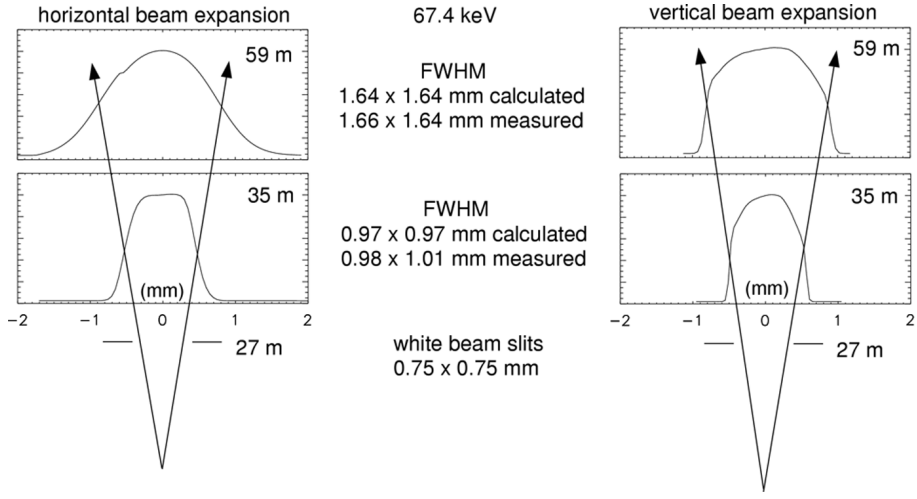

Figure 3
Measurements at 67 keV of horizontal (left) and vertical (right) beam profiles at 35 and 59 m from the source, made to ascertain unperturbed linear (brilliance-preserved) beam expansion after the double-Laue premonochromator located at 32 m. The defining white-beam slits were at 27 m.

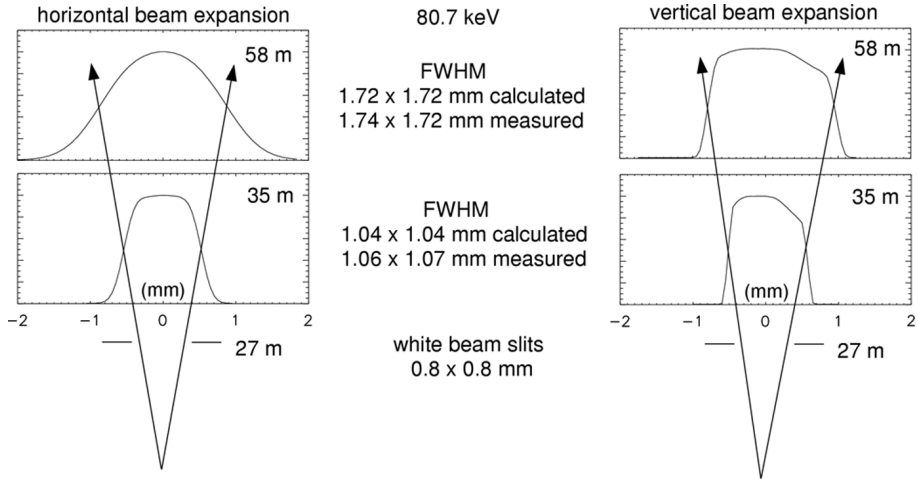

Figure 4
Measurements at 81 keV of horizontal (left) and vertical (right) beam profiles at 35 and 58 m from the source, made to ascertain unperturbed linear (brilliance-preserved) beam expansion after the double-Laue premonochromator located at 32 m. The defining white-beam slits were at 27 m.

at 67 and 81 keV, respectively. At 67 keV, for example, setting the white-beam slits positioned at 27 m to define a square aperture of dimensions 0.75 × 0.75 mm produced monochromatic beam sizes of 1.0 × 1.0 mm at 35 m and 1.6 × 1.6 mm at 59 m, in nearly exact agreement with the distance ratios. This simple test offers evidence of ray divergence preservation at the few microradian level, a property that enables the successful further collimation (or focusing) of the premonochromatized beam by CRLs or other devices.

3. Collimation with CRLs

Achieving high energy resolution in X-ray optics using the two-stage monochromatization scheme has already been exploited to deliver meV-bandwidth beams at lower energies ($E < 25$ keV) for inelastic scattering and nuclear resonance scattering (Toellner *et al.*, 1993; Toellner, 2000). In such cases, the intrinsically low divergence of the central radiation cone from a low-order odd harmonic of an undulator source often falls completely or mostly within the angular acceptance of not only the premonochromator but also the high-resolution monochromator because of widened acceptances from asymmetric Bragg crystal orientations or near-backscattering geometries. At high energies, however, flat crystal acceptances become narrower, and asymmetrical orientation and backscattering are not as effective. Furthermore, the sources often used here are wigglers, which have substantial divergences. Even in this study, where an APS undulator A source was used, the slight insertion-device magnetic-field errors and particle-beam energy spread give rise to strong wiggler-like behavior at high photon energies $E > 50$ keV (Shastri *et al.*, 1998) and hence larger divergences of order $1/\gamma$ (tens of microradians), where γ is the relativistic parameter. [APS undulator A is a 3.3 cm-period device with 70 planar periods and a deflection parameter $k = 2.7$ at the minimum 11 mm gap, operating in a 7 GeV storage ring (Lai *et al.*, 1993; Dejus *et al.*, 1994, 2002).] For these reasons, the placement of a collimating optic between the two monochromators is highly beneficial.

Having established in the preceding section that the bent Laue crystals preserve the ray propagation from the source, the successful vertical angular collimation of this beam by CRLs is shown in this section, after a brief explanation of CRL operation with X-rays. In the case of visible light, whose phase velocity is slower in glass than in a vacuum or air, convex glass lenses have a focusing effect. For X-rays, however, whose phase velocity in materials is faster than in a vacuum/air, focusing is achieved by concave elements. A series of concave lenses can be produced, for example, by drilling a closely spaced linear array of small cylindrical holes in a material, leaving thin concave separating walls. An X-ray beam sent through all the thin walls will experience one-dimensional focusing in the plane normal to the cylinders' axes, demonstrating a basic version of the CRL concept. A sketch of the type of CRLs used here (from Adelphi Technology Inc., Palo Alto, CA, USA, http://www.adelphitech.com) is shown in Fig. 2. The focal length of such a device is given by $f = R/2N\delta$, where R is the wall curvature radius, N is the number of wall elements, and $\delta = 1 - n$ quantifies the decrement of the material's refractive index from unity. For low-energy X-rays (*e.g.* 10 keV), low-absorption materials like Be are best for CRLs. At the high energies of relevance here, the incremental performance of Be over that of the heavier and more convenient material Al is marginal because of the reduced disparity between their attenuations and the higher electron density (refractive strength) of Al. The Al CRLs used here have cylindrical elements, whereas the optimal profile for aberration-free collimation and focusing is parabolic.

The CRLs were placed at a distance of 35 m from the source, just after the bent double-Laue monochromator, and oriented for vertical collimation. At this location, the desired collimating action corresponds to a focal length $f = 35$ m, which is achieved for 67 keV X-rays by 60 elements of 1 mm diameter. For 81 keV X-rays, 86 such elements are required. The CRLs used had approximately 20–50 μm wall thicknesses. Fig. 5 displays beam profiles indicating how the vertical beam propagation was influenced by the CRLs at 67 and 81 keV. Although the beam size on the CRLs was 1.0 × 1.0 mm, the changing attenuation along the curved CRL walls gave rise to an effective vertical aperture that resulted in a 50% transmitted beam of 0.5 mm FWHM vertical size. However, in sharp contrast to the linear beam expansion behavior reported in Figs. 3 and 4, here the vertical beam size of 0.5 mm remained preserved in propagation from the CRL to the beamline end-station at roughly 60 m from the source. This result is evidence of vertical collimation to a few microradians. That the collimation achieved was good, but not perfect, is suggested in Fig. 5, which shows the interesting behavior of the beam transforming from a Gaussian to a square shape in free-space propagation from just after the CRL to the end-station. Finally, we should not expect the CRLs to affect ray propagation in the horizontal plane. This claim was confirmed by checking that the horizontal beam profiles (not shown) were unchanged from those on the left-side panels in Figs. 3 and 4. Although the technique used here of measuring beam profiles at separate locations is not an extremely sensitive method of collimation or divergence measurement (for

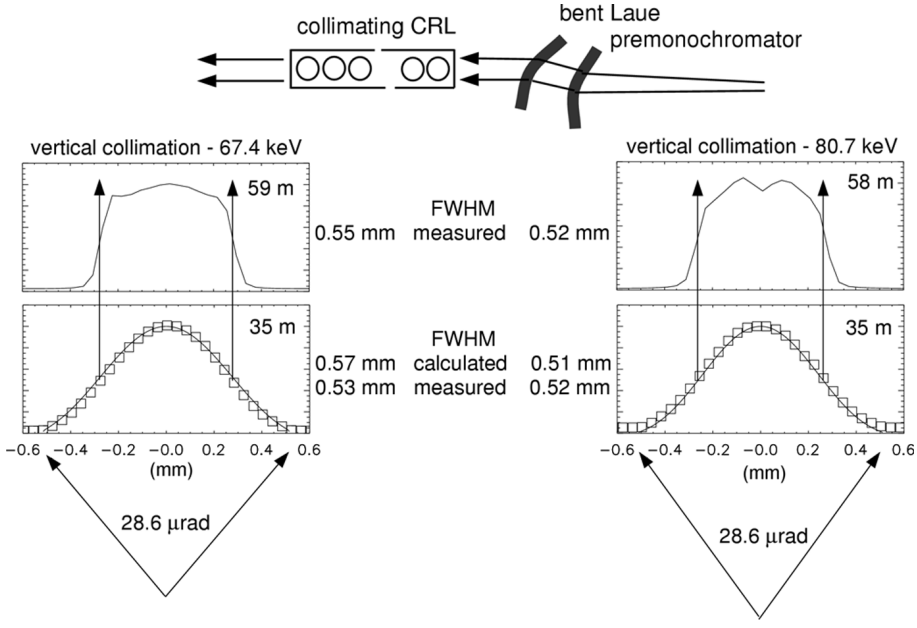

Figure 5
Measurements, taken at 67 keV (left) and 81 keV (right), of vertical beam profiles at 35 m (immediately after the CRL) and ∼60 m from the source, made to ascertain the vertical angular collimation achieved by the CRLs from 29 μrad to a few microradians. All plotted profiles are measured ones, except for the solid lines in the two lower 35 m panels, which are calculated (square symbols are used for measurements here).

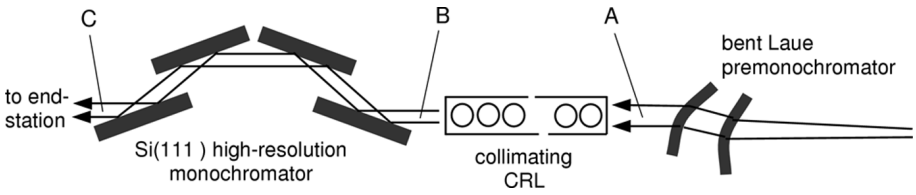

Figure 6
Depiction of the post-monochromatization scheme starting with the bent double-Laue premonochromator, which is then followed by a collimating CRL and the four-reflection flat-crystal high-resolution monochromator. Beam properties at the locations labeled *A*, *B* and *C* are analyzed in the text and in Tables 1 and 2.

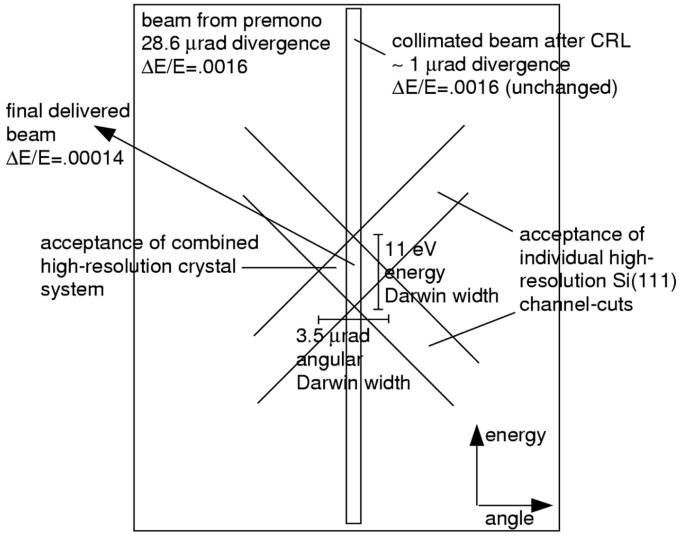

Figure 7
Dumond diagram representation (energy *versus* vertical angle) for 81 keV X-rays at various steps of propagation, starting just after the premonochromator and then passing through the collimating CRL and four-reflection high-resolution monochromator, assuming ideal performance of the optics shown in Fig. 6.

1 μrad sensitivity or better, achievable with crystal analyzers or transmission images of test patterns), it suffices at the level of a few μrad.

4. High-energy-resolution system performance

Having collimated the premonochromatized beam with a CRL, we can then deliver it through the narrow-angular-acceptance high-resolution monochromator composed of four symmetric Si(111) crystal reflections arranged to resemble two channel cuts in a dispersive $(+--+)$ arrangement (Fig. 6). As explained in more detail below, depending on the degree of collimation, this step results in a final monochromatization level of between one-half and one times the Si(111) intrinsic bandwidth (*i.e.* energy Darwin width), $(\delta E/E)_{111} = 1.4 \times 10^{-4}$. In principle, since the beam is collimated, only one reflection, instead of four, would suffice to monochromatize to this level. However, a single-reflection scheme suffers from two problems. First, the exit beam would not emerge parallel to the incident beam, and second, angular instabilities in the incident beam (arising from either the premonochromator or the storage ring) would lead to energy as well as angular drifts in the final beam. Adding a second reflection to form a double-reflection $(+-)$ geometry resembling a single channel-cut crystal would address the first problem but not the second. The full four-reflection setup employed here not only restores the beam propagation direction but also establishes a well defined selection window in both energy and angle that is extremely stable as a result of its operation in an ambient room environment, which, unlike that of the premonochromator, is essentially perturbation free. The result is a final delivered beam that is drift-free in energy and vertical angle (although perhaps not in intensity), regardless of any fluctuations upstream of the high-resolution monochromator.

The statements in the previous paragraph are clarified by the Dumond representation in Fig. 7. Dumond diagrams offer a convenient graphical means of visualizing the evolution of the two-dimensional distribution, in angle and energy, of a ray ensemble of photons undergoing multiple Bragg reflections through a sequence of flat perfect crystals (Dumond, 1937). The diagram in Fig. 7 specifically depicts this beam evolution as theoretically expected for the case of 81 keV X-rays passing through the optics considered here, assuming ideal performance. The large outer rectangle represents the beam, after the premonochromator, that is incident on the CRL. This radiation is characterized by a bandwidth $\Delta E/E = 1.6 \times 10^{-3}$ and a vertical divergence of 29 μrad, associated with a 1 mm beam size on the CRL located 35 m from the source. In passing through the collimating CRL, the bandwidth is unchanged; however, the divergence is drastically reduced to 1 μrad or so (even with ideal optics, the non-zero source size precludes perfect collimation), and so the Dumond profile of the collimated X-rays is given by the thin vertical rectangle. That the collimation process is lossy (50% attenuation in the CRL) is information unrecorded in the Dumond diagram and must therefore be kept in mind for the overall efficiency assessment. Fig. 7 also contains two diagonal strips. The diagonal strip of positive slope defines all the rays of energy and angle that would be accepted through the first flat-crystal pair with near unit reflectivity. This strip is simply constructed to have a slope consistent with the linearization of Bragg's law in the vicinity of the energy of interest and to have a width which, taken parallel to the angle axis (abscissa), is the angular Darwin width [*i.e.* 3.5 μrad for Si(111) at 81 keV]. The other strip, which represents the acceptance band of the second crystal pair, has its slope reversed, because rays traveling through the first crystal pair with higher incidence angles reach the second pair with lower incidence angles. The intersection of the two diagonal strips forms a diamond-shaped region that represents the fixed energy–angle acceptance window defined by the four-reflection high-resolution system. Finally, the intersection of this small window with the narrow vertical rectangle shows the photons exiting the high-resolution system, which would theoretically have an 11 eV energy spread $(\Delta E/E = 1.4 \times 10^{-4})$. At this point, it is clear that an angular drift in the beam entering this system, manifested in the Dumond diagram as an overall horizontal shifting of the narrow vertical rectangle, leaves the mean energy of the final beam's spectral profile unchanged. This would not be the case for the X-rays just after the first crystal pair.

From the analysis above, the expected ratio of final flux to that just after the premonochromator is simply the product of the roughly one-tenth bandwidth reduction and the one-half transmission through the CRL, together amounting to approximately $(10^{-4}/10^{-3})(50\%) = 1/20$. A more precise calculation predicts $(0.00014/0.0013)(53\%) = 1/18$ and $(0.00014/0.0016)(50\%) = 1/23$ for 67 and 81 keV photon energies, respectively. The photon fluxes measured at various points in the setup are summarized in Tables 1 and 2 for the two X-ray energies. These tables also give the beam sizes

Table 1
Tabulation of actual beam characteristics (distance from souce, size, flux, and bandwidth) for 67 keV X-rays at various stages through the optics.

The locations *A*, *B* and *C* are labeled in Fig. 6. Location *D* is at the line focus created by an additional focusing CRL placed after the high-resolution monochromator, as depicted in Fig. 10.

Location, distance from source	Beam size $h \times v$ FWHM (mm^2)	Flux (photons s^{-1})	Energy width FWHM	
			ΔE (eV)	$\Delta E/E$
A, 32 m	1×1	$I_0 = 4.0 \times 10^{12}$	90	1.3×10^{-3}
B, 35 m	1×0.5	$I_0/1.9$	90	1.3×10^{-3}
C, 36 m	1×0.5	$I_0/33.5 = 1.2 \times 10^{11}$	5	7×10^{-5}
D, 60 m	1.6×0.067	$I_0/57.9 = 6.9 \times 10^{10}$	5	7×10^{-5}

Table 2
Tabulation of actual beam characteristics (distance from source, size, flux, and bandwidth) for 81 keV X-rays at various stages through the optics.

The locations *A*, *B* and *C* are labeled in Fig. 6.

Location, distance from source	Beam size $h \times v$ FWHM (mm^2)	Flux (photons s^{-1})	Energy width FWHM	
			ΔE (eV)	$\Delta E/E$
A, 32 m	1×1	$I_0 = 4.0 \times 10^{12}$	127	1.6×10^{-3}
B, 35 m	1×0.5	$I_0/2$	127	1.6×10^{-3}
C, 36 m	1×0.5	$I_0/52 = 7.7 \times 10^{10}$	6.0	7.4×10^{-5}

and energy spreads at the various locations. Instead of the expected 1/18 and 1/23 flux drops through the CRL/flat-crystal system, reductions of 1/34 and 1/52 were measured at the two photon energies – a discrepancy factor of about two. This result could reasonably be ascribed to imperfect collimation by the CRL (beyond the source-size effect), a consequence that is expected because its elements have cylindrical profiles as opposed to the optimal parabolic shape. A possible additional smaller contribution to imperfect collimation is a slight mismatch of the number of elements to the distance from the source. The twofold discrepancy corresponds to a residual divergence of 3–4 μrad, which would be represented by a Dumond diagram slightly altered from that in Fig. 7, by having the collimated beam's angular profile extend approximately from the left to the right vertices of the flat crystals' acceptance window (one angular Darwin width). Then, only half the collimated radiation within the Si(111)-energy Darwin width is accepted.

Despite the CRL collimation performance being imperfect, it still significantly enhances the output of the full system. Again, for a moment considering the ideal optics situation, removing the CRL should result in a very large eightfold loss in the final flux, even with the eliminated CRL attenuation. This factor of eight is the divergence ratio of the uncollimated beam to the mean angular acceptance of the high-resolution Dumond window (one-half the angular Darwin width), multiplied by the CRL transmission, which gives 29 μrad/[(1/2)(3.5 μrad)] × 50% = 8.3 for the 81 keV case. For 67 keV X-rays, where the angular Darwin width is 4.1 μrad, the insertion of the CRL should increase the final flux by a factor of 29 μrad/[(1/2)(4.1 μrad)] × 53% = 7.5. In reality, the measured flux enhancement due to the CRL was very close to fourfold at both energies, again revealing the same discrepancy factor of two as the analysis in the previous paragraph.

Interestingly, the overall factor of two in flux underperformance, which has been attributed to imperfect angular collimation, should result in improved (narrower) energy resolution in the final beam. Since the imperfectly collimated beam illuminates the full Dumond acceptance window of the flat-crystal system (Fig. 7), the final energy spectrum is not a square function with a width of one energy Darwin width, as proposed earlier, but a triangular function whose FWHM is one-half that value, *i.e.* $\Delta E/E = 7 \times 10^{-5}$. This fact was verified for the setup at 81 keV by analyzing the energy spread by scanning a high-order Si(777) reflection through the final beam and measuring $\Delta E = 6.0$ eV FWHM, equivalent to $\Delta E/E = 7.4 \times 10^{-5}$. Based on this reasoning, at 67 keV, we would expect a reduced energy spread of 5 eV (not verified). Also worth noting is that the slight amount of imperfect collimation encountered here (residual divergence comparable to the angular Darwin width) is just enough to taper the square energy-resolution spectral profile to a triangular one, whose central photon energy is still fully transmitted through the flat crystals. This is fortuitously beneficial for some experiments, such as nuclear resonance scattering, wherein the resonant signal is unchanged but non-resonant noise is reduced if the system is carefully set to have the resonance coincide with the resolution function peak.

Mentioning some details about the mechanical implementation of the high-resolution four-crystal monochromator is in order. Each parallel crystal pair was not a true channel-cut device (*i.e.* referring to the scheme in which a slot is cut through a single monolithic piece of silicon) but consisted of two separate crystals attached to an aluminium plate, which was in turn mounted on a rotation stage. The high-resolution monochromator is composed of two such assemblies. The fine adjustment of parallelism between the two crystals of one pair was achieved by a flexure mechanism, where the controlled elastic deflection of a weak link in the aluminium plate was induced by a linear picomotor actuator pushing through a compression spring. The result was a mechanical displacement demagnification with a nearly constant force and a good stability, with 1 μm of picomotor travel giving 60 nrad relative angular deflection. There are various reasons for not using monolithic channel cuts. The desire for flexibility in using the system over a wide energy range (50–100 keV) would have resulted in a somewhat complicated channel-cut crystal design with the technical problem of polishing the inside surfaces of the slots. Intrinsic sub-microradian strain misalignment between the faces of the two reflecting slabs would also be a concern. Instead, the employed configuration of separate crystals on a flexure requires simply fabricated crystal blocks that are easily repositioned on the plate to accommodate the different ray traces at different energies.

Scanning the high-resolution monochromator in energy is accomplished by rotating the two crystal pairs in opposite directions by the same amount. In the Dumond picture (Fig. 7), this process corresponds to a vertical displacement of the acceptance window. The resolution/repeatability of the two rotation stages has to be sufficiently good, *i.e.* around a few hundred nanoradians. A slight difference in the step size of the two rotations results in the Dumond window displacing horizontally, and we can start losing the collimated beam through the high-resolution crystals. The Huber 410 stages used here, although operated with gear-reduction and microstepped motors, did not quite have the required level of angular precision, which lies slightly beyond their specifications. However, they sufficed for a test of the optics. Fig. 8 shows the attenuation of a pure 100 μm-thick Ta foil in the vicinity of its *K*-edge at 67.4 keV, as measured with both the modest-energy-resolution (90 eV) and the high-energy-resolution (5 eV) beams. Also plotted is the 90 eV-wide output spectral profile of the premonochromator, measured by scanning the high-resolution monochromator in energy, keeping the premonochromator fixed.

5. Focusing with CRLs

Having presented the main concept of this article in the previous section, namely the bent Laue premonochromator/collimating CRL/high-resolution monochromator combination scheme for high-energy X-ray optics, this section briefly describes some simple configurational variants incorporating focusing with CRLs. This discussion does not refer to microfocusing (*i.e.* to ∼μm size spots) but rather to focusing to sub-100 μm dimensions, which is very effectively achieved with CRLs having focal lengths of tens of meters placed at roughly 1:1 source–demagnification geometries. Although microfocused spots at high energies can be obtained with CRLs, the significant attenuation due to the large number (thousands) of wall elements required for ∼1 m focal lengths makes the process inefficient.

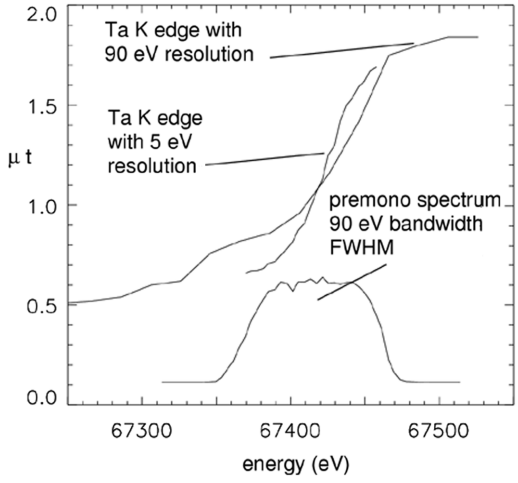

Figure 8
K-edge attenuation (*i.e.* negative logarithm of measured transmission) of a Ta foil of thickness $t = 100$ μm, measured with both the premonochromatized X-rays and the high-resolution X-rays. The high-resolution monochromator selected a narrow 5 eV-wide slice out of the broader 90 eV bandwidth profile (also shown) exiting the premonochromator.

As the first example, creating a line focus of broad bandwidth in the end-station 60 m from the source was attempted by placing a CRL at 36 m, a few meters after the double-Laue monochromator at 32 m (see Fig. 9). This setup corresponds to a 1:0.7 source demagnification, requiring 147 and 211 CRL elements for 67 and 81 keV X-rays, respectively (still using 1 mm-diameter cylindrical walls in Al). Line-focus profiles (shown in Fig. 9) of 70–90 μm height FWHM were measured, approximately twice the value expected from the vertical electron beam size and ideal demagnification. The discrepancy can be reasonably attributed to cylindrical aberration in the CRLs. Removing the CRL results in an end-station vertical beam size of 1.6–1.7 mm (right panels of Figs. 3 and 4). The factor of 20 reduction in vertical beam size is accompanied by a 30% CRL transmission, amounting to flux-density gains of about 6. This enhancement has been exploited in high-energy X-ray small-angle scattering applications (Almer *et al.*, 2003), where a two-dimensional detector is positioned at the focal location.

The second example is a hybrid of that just presented (Fig. 9) and of the high-energy-resolution setup (Fig. 6) discussed in depth in §4. This hybrid is realized by the addition of a second CRL, just after the flat crystals (at 36 m from the source), in order to obtain a line-focused narrow-bandwidth beam in the 60 m end-station (Fig. 10). Here, the sum of the numbers of elements in both CRLs should equal that required for 1:0.7 source demagnification, appropriately partitioned so that the first CRL accomplishes its collimation task. Such a setup was tested at 67 keV, attaining a line focus whose vertical profile (67 μm FWHM) was unchanged from that measured in the broader bandwidth configuration (Fig. 9). Without the second CRL, a vertically collimated beam propagates to the end-station with an essentially unchanging vertical size of 0.5 mm FWHM (Fig. 5). The size reduction from 0.5 mm to 67 μm, combined with the 58% transmission due to the added CRL, represents a flux-density gain of about a factor of 4 in this narrow-bandwidth mode. The properties of the final narrow-bandwidth line-focused beam are given in the bottom row of Table 1. Although the beam had to pass through many more walls in the second CRL (90 elements) than in the first (60 elements), the transmission through the second CRL is greater than the 53% transmission of the first, because the attenuation profile of the first CRL's walls effectively apertures the beam vertically from 1 to 0.5 mm (Fig. 5), subjecting the second CRL to fewer off-plane rays.

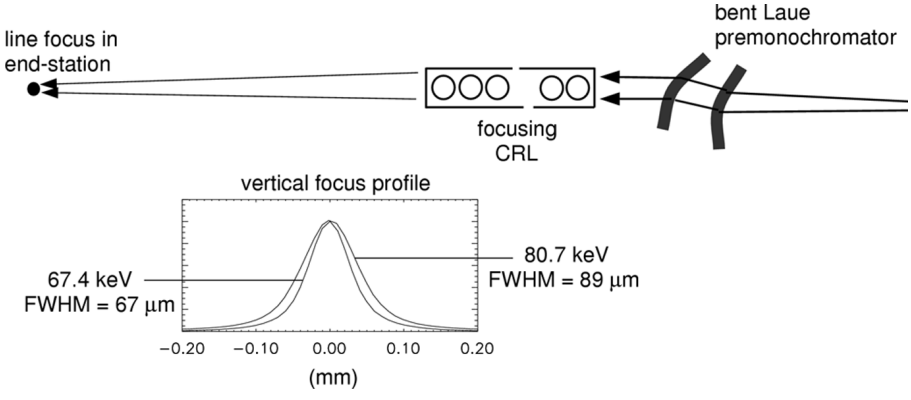

Figure 9
Arrangement producing a line focus with a CRL and just the double-Laue monochromator. Vertical beam profiles are shown for tests with 67 and 81 keV X-rays. The demagnification ratio is 1:0.7.

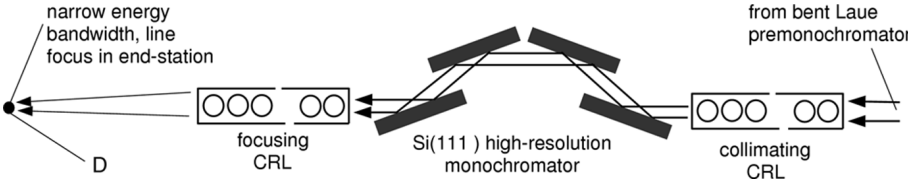

Figure 10
Placement of an additional focusing CRL after the high-resolution monochromator produces a line focus of photons with narrow bandwidth in the end-station with a 1:0.7 source–demagnification geometry. Properties at the line-focus position (labeled *D*) are given in Table 1.

Focusing the beam horizontally with CRLs, in addition to vertically, was not attempted as it is not worthwhile considering the relatively large horizontal source size (600–800 μm), CRL attenuation, and limited CRL spatial aperture. The flux density of the horizontally unfocused beam in the end-station is comparable to, if not more than, that offered by horizontally focusing CRLs.

However, horizontal focusing can provide significant flux-density gains if large-spatial-acceptance (> 5 mm) focusing optics can be used, capturing more of the wide wiggler-like radiation fan coming from APS undulator A at high energies (Shastri *et al.*, 1998).

6. Concluding remarks

This article has demonstrated a highly efficient and effective method of implementing optics for a high-energy X-ray beamline by combining flat and bent crystals and CRLs. We start with a bent double-Laue monochromator that provides high flux and a 10^{-3} bandwidth, which is suitable for most experiments. In addition to offering a tunable in-line system, this monochromator preserves beam divergence and size, allowing flexible schemes for further beam conditioning with high throughput using subsequent optics. For example, higher energy resolution (10^{-5} levels) was achieved by passing the beam through a collimating CRL and a four-reflection flat-crystal high-resolution monochromator. Vertical focusing with CRLs can be integrated into both the modest- and the high-resolution configuration. By keeping the cryogenically cooled first monochromator invariant and relegating the task of high-resolution monochromatization to downstream optics, we reduce complexity at the high-heat-load (white-beam) stage and allow the downstream optics to function in an unperturbed stable environment. For a multipurpose high-energy beamline, the reasons above make such an approach advantageous over one where the white beam is passed first through a collimating CRL and then through a standard flat double-crystal monochromator.

Various improvements can be pursued for the optics described. In addition to the vertical focusing accomplished by the CRLs, we can attempt to incorporate horizontal focusing by superimposing the appropriate sagittal bending upon the asymmetric Laue crystals, which are already meridionally bent to meet Rowland conditions (Zhong *et al.*, 2001*a*,*b*). A second improvement is to have a variable-focal-length feature for the CRLs. This is straightforward to achieve, and has been implemented for the collimating CRL by having many devices of increasing numbers of elements stacked next to one another. A horizontal motion adds or removes elements in the beam. This simple arrangement is essential not only for energy tunability but also for optimizing the beam collimation empirically, thereby compensating for unknown factors affecting focal length, such as exact CRL wall figure, refractive index of impurities, and effective distance to the source. Using materials lighter than aluminium at high energies can give marginal, but perhaps worthwhile, throughput increases. However, a more important enhancement for improved collimation and focusing would be the use of aberration-free one-dimensional parabolically shaped CRLs, as opposed to the cylindrical ones used here. Such devices are being developed using materials suitable for high energies, such as silicon (Cederström *et al.*, 2002; Snigireva *et al.*, 2002) and aluminium (Khounsary *et al.*, 2002). The single-crystal silicon CRLs are particularly interesting in that they offer reduced small-angle scattering surrounding the collimated or focused beam. Finally, note that there is a substantial parameter space over which the high-resolution monochromator can be optimized to match the experimental application of interest, by tuning the reflection orders and asymmetries of the flat crystals. Efficient monochromatization to bandwidths of a few meV in the 50–100 keV energy range (as would be required for exciting various nuclear resonances) would need nanoradian angular control and cryogenic stabilization of the high-resolution silicon crystal optics (Toellner, 2003).

The assistance of A. Mashayekhi at the XOR 1-ID beamline is acknowledged, along with the technical cooperation of Adelphi Technology Inc., Palo Alto, CA, USA, in manufacturing the aluminium CRLs. Use of the APS is supported by the US Department of Energy, Office of Science, Basic Energy Sciences, under contract No. W-31-109-Eng-38.

References

Almer, J. D. *et al.* (2003). To be published.
Badyal, Y. S., Price, D. L., Saboungi, M. L., Haeffner, D. R. & Shastri, S. D. (2002). *J. Chem. Phys.* **116**, 10833–10837.
Badyal, Y. S., Saboungi, M.-L., Price, D. L., Haeffner, D. R. & Shastri, S. D. (1997). *Europhys. Lett.* **39**, 19–24.
Baron, A. Q. R., Kohmura, Y., Ohishi, Y. & Ishikawa, T. (1999). *Appl. Phys. Lett.* **74**, 1492–1494.
Cederström, B., Lundqvist, M. & Ribbing, C. (2002). *Appl. Phys. Lett.* **81**, 1399–1401.
Curry, J. J., Adler, H. G., Shastri, S. D. & Lawler, J. E. (2001). *Appl. Phys. Lett.* **79**, 1974–1976.
Curry, J. J., Adler, H. G., Shastri, S. D. & Lee, W.-K. (2003). *J. Appl. Phys.* **93**, 2359–2368.
Dejus, R. J., Lai, B., Moog, E. R. & Gluskin, E. (1994). Report ANL/APS/TB-17. Argonne National Laboratory, IL 60439, USA.
Dejus, R. J., Vasserman, I. B., Sasaki, S. & Moog, E. R. (2002). Report ANL/APS/TB-45. Argonne National Laboratory, IL 60439, USA.
Dumond, J. W. M. (1937). *Phys. Rev.* **52**, 872–883.
Khounsary, A., Shastri, S. D., Mashayekhi, A., Macrander, A. T., Smither, R. K. & Kraft, F. F. (2002). *Proc. SPIE*, **4783**, 49–54.
Kramer, M. J., Margulies, L., Goldman, A. I. & Lee, P. L. (2002). *J. Alloys Compd.* **338**, 235–241.
Lai, B., Khounsary, A., Savoy, R., Moog, E. & Gluskin, E. (1993). Report ANL/APS/TB-3. Argonne National Laboratory, IL 60439, USA.
Lengeler, B., Schroer, C., Tümmler, J., Benner, B., Richwin, M., Snigirev, A., Snigireva, I. & Drakopoulos, M. (1999). *J. Synchrotron Rad.* **6**, 1153–1167.
Lienert, U., Keitel, S., Caliebe, W., Schulze-Briese, C. & Poulsen, H. F. (2001). *Nucl. Instrum. Methods Phys. Res. A*, **467**, 659–662.
Petkov, V., Billinge, S. J. L., Shastri, S. D. & Himmel, B. (2000). *Phys. Rev. Lett.* **85**, 3436–3439.
Petkov, V., Billinge, S. J. L., Shastri, S. D. & Himmel, B. (2001). *J. Non-Cryst. Solids*, **293/295**, 726–730.
Shastri, S. D., Dejus, R. J. & Haeffner, D. R. (1998). *J. Synchrotron Rad.* **5**, 67–71.
Shastri, S. D., Fezzaa, K., Mashayekhi, A., Lee, W.-K., Fernandez, P. B. & Lee, P. L. (2002). *J. Synchrotron Rad.* **9**, 317–322.
Shastri, S. D., Shu, D., Zhang, Y., Lee, P. L. & Wilkinson, A. P. (2004). To be published.
Snigirev, A., Kohn, V., Snigireva, I. & Lengeler, B. (1996). *Nature* (*London*), **384**, 49–51.
Snigireva, I., Grigoriev, M., Shabel'nikov, L., Yunkin, V., Snigirev, A., Kuznetsov, S., Di Michiel, M., Hoffman, M. & Voges, E. (2002). *Proc. SPIE*, **4783**, 19–27.
Suortti, P. & Schulze, C. (1995). *J. Synchrotron Rad.* **2**, 6–12.
Toellner, T. S. (2000). *Hyperfine Interact.* **125**, 3–28.
Toellner, T. S. (2003). Personal communication.
Toellner, T. S., Mooney, T. M., Shastri, S. D. & Alp, E. E. (1993). *Proc. SPIE*, **1740**, 218–223.
Wang, Y. D., Wang, X.-L., Stoica, A. D., Almer, J. D., Lienert, U. & Haeffner, D. R. (2002). *J. Appl. Cryst.* **35**, 684–688.
Welberry, T. R., Goossens, D. J., Haeffner, D. R., Lee, P. L. & Almer, J. (2003). *J. Synchrotron Rad.* **10**, 284–286.
Wilkinson, A. P., Lind, C., Young, R. A., Shastri, S. D., Lee, P. L. & Nolas, G. S. (2002). *Chem. Mater.* **14**, 1300–1305.
Zhong, Z., Kao, C. C., Siddons, D. P. & Hastings, J. B. (2001*a*). *J. Appl. Cryst.* **34**, 504–509.
Zhong, Z., Kao, C. C., Siddons, D. P. & Hastings, J. B. (2001*b*). *J. Appl. Cryst.* **34**, 646–653.